Scattering efficiency and near field enhancement of active semiconductor plasmonic antennas at terahertz frequencies

Vincenzo Giannini,[1*] Audrey Berrier,[1] Stefan A. Maier,[2] José Antonio Sánchez-Gil,[3] and Jaime Gómez Rivas[1]

[1]*FOM Institute for Atomic and Molecular Physics AMOLF, c/o Philips Research Laboratories, High Tech Campus 4, 5656 AE, Eindhoven, The Netherlands.*
[2]*Experimental Solid State Group, Physics Department, Imperial College London, London SW7 2AZ, UK.*
[3]*Instituto de Estructura de la Materia, Consejo Superior de Investigaciones Científicas, Serrano 121, 28006 Madrid, Spain.*
*giannini@amolf.nl

Abstract: Terahertz plasmonic resonances in semiconductor (indium antimonide, InSb) dimer antennas are investigated theoretically. The antennas are formed by two rods separated by a small gap. We demonstrate that, with an appropriate choice of the shape and dimension of the semiconductor antennas, it is possible to obtain large electromagnetic field enhancement inside the gap. Unlike metallic antennas, the enhancement around the semiconductor plasmonics antenna can be easily adjusted by varying the concentration of free carriers, which can be achieved by optical or thermal excitation of carriers or electrical carrier injection. Such active plasmonic antennas are interesting structures for THz applications such as modulators and sensors.

References and links

1. K. H. Yang, P. L. Richards, and Y. R. Shen, "Generation of far-infrared radiation by picosecond light pulses in LiNbO$_3$," Appl. Phys. Lett. **19**(9), 320–323 (1971).
2. D. H. Auston, A. M. Glass, and A. A. Ballman, "Optical Rectification by Impurities in Polar Crystals," Phys. Rev. Lett. **28**(14), 897–900 (1972).
3. Terahertz Spectroscopy, *Principles and Applications*, S.L. Dexheimer (ed.) (CRC Press, 2008).
4. J. Saxler, J. Gómez Rivas, C. Janke, H. P. M. Pellemans, P. Haring Bolivar, and H. Kurz, "Time domain measurements of surface plasmon polaritons in the terahertz frequency range," Phys. Rev. B **69**(15), 155427 (2004).
5. D. Qu, D. Grischkowsky, and W. Zhang, "Terahertz transmission properties of thin, subwavelength metallic hole arrays," Opt. Lett. **29**(8), 896–898 (2004).
6. K. Wang, and D. M. Mittleman, "Metal wires for terahertz wave guiding," Nature **432**(7015), 376–379 (2004).
7. H. Cao, and A. Nahata, "Resonantly enhanced transmission of terahertz radiation through a periodic array of subwavelength apertures," Opt. Express **12**(6), 1004–1010 (2004).
8. A. Rusina, M. Durach, K. A. Nelson, and M. I. Stockman, "Nanoconcentration of terahertz radiation in plasmonic waveguides," Opt. Express **16**(23), 18576–18589 (2008).
9. M. A. Seo, H. R. Park, S. M. Koo, D. J. Park, J. H. Kang, O. K. Suwal, S. S. Choi, P. C. M. Planken, G. S. Park, N. K. Park, Q. H. Park, and D. S. Kim, "Terahertz field enhancement by a metallic nano slit operating beyond the skin-depth limit," Nat. Photonics **3**(3), 152–156 (2009).
10. S. A. Maier, "Plasmonics: Fundamentals and Applications," Springer, (2007).
11. J. Gómez Rivas, "THz: The art of confinement," Nat. Photonics **2**(3), 137–138 (2008).
12. R. Ulrich, and M. Tacke, "Submillimeter waveguiding on periodic metal structure," Appl. Phys. Lett. **22**(5), 251–253 (1973).
13. D. L. Mills, and A. A. Maradudin, "Surface corrugation and surface-polariton binding in the infrared frequency range," Phys. Rev. B **39**(3), 1569–1574 (1989).
14. J. B. Pendry, L. Martín-Moreno, and F. J. Garcia-Vidal, "Mimicking surface plasmons with structured surfaces," Science **305**(5685), 847–848 (2004).
15. H. Cao, and A. Nahata, "Coupling of terahertz pulses onto a single metal wire waveguide using milled grooves," Opt. Express **13**(18), 7028–7034 (2005).

16. A. P. Hibbins, B. R. Evans, and J. R. Sambles, "Experimental verification of designer surface plasmons," Science **308**(5722), 670–672 (2005).
17. S. A. Maier, S. R. Andrews, L. Martin-Moreno, and F. J. Garcia-Vidal, "Terahertz surface plasmon-polariton propagation and focusing on periodically corrugated metal wires," Phys. Rev. Lett. **97**(17), 1–4 (2006).
18. C. R. Williams, S. R. Andrews, S. A. Maier, A. I. Fernández-Domínguez, L. Martín-Moreno, and F. J. García-Vidal, "Highly confined guiding of terahertz surface plasmon polaritons on structured metal surfaces," Nat. Photonics **2**(3), 175–179 (2008).
19. J. G. Rivas, M. Kuttge, P. H. Bolivar, H. Kurz, and J. A. Sánchez-Gil, "Propagation of surface plasmon polaritons on semiconductor gratings," Phys. Rev. Lett. **93**(25), 256804 (2004).
20. R. Parthasarathy, A. Bykhovski, B. Gelmont, T. Globus, N. Swami, and D. Woolard, "Enhanced Coupling of Subterahertz Radiation with Semiconductor Periodic Slot Arrays," Phys. Rev. Lett. **98**(15), 153906 (2007).
21. J. G. Rivas, P. H. Bolivar, and H. Kurz, "Thermal switching of the enhanced transmission of terahertz radiation through sub-wavelength apertures," Opt. Lett. **29**(14), 1680–1682 (2004).
22. C. Janke, J. G. Rivas, P. H. Bolivar, and H. Kurz, "All-optical switching of the transmission of electromagnetic radiation through subwavelength apertures," Opt. Lett. **30**(18), 2357–2359 (2005).
23. C. L. Pan, C. F. Hsieh, R. P. Pan, M. Tanaka, F. Miyamaru, M. Tani, and M. Hangyo, "Control of enhanced THz transmission through metallic hole arrays using nematic liquid crystal," Opt. Express **13**(11), 3921–3930 (2005).
24. W. Zhang, A. K. Azad, J. Han, J. Xu, J. Chen, and X.-C. Zhang, "Direct observation of a transition of a surface plasmon resonance from a photonic crystal effect," Phys. Rev. Lett. **98**(18), 183901 (2007).
25. H.-T. Chen, H. Lu, A. K. Azad, R. D. Averitt, A. C. Gossard, S. A. Trugman, J. F. O'Hara, and A. J. Taylor, "Electronic control of extraordinary terahertz transmission through subwavelength metal hole arrays," Opt. Express **16**(11), 7641–7648 (2008).
26. E. Hendry, F. J. Garcia-Vidal, L. Martin-Moreno, J. Gómez Rivas, M. Bonn, A. P. Hibbins, and M. J. Lockyear, "Optical control over surface plasmon polariton-assisted THz transmission through a slit aperture," Phys. Rev. Lett. **100**(12), 123901 (2008).
27. J. Gómez Rivas, M. Kuttge, H. Kurz, P. Haring Bolivar, and J. A. Sánchez-Gil, "Low-frequency active surface plasmon optics on semiconductors," Appl. Phys. Lett. **88**(8), 082106 (2006).
28. J. A. Sánchez-Gil, and J. Gómez Rivas, "Thermal switching of the scattering coefficients of terahertz surface plasmon polaritons impinging on a finite array of subwavelength grooves on semiconductor surfaces," Phys. Rev. B **73**(20), 205410 (2006).
29. J. Gómez Rivas, J. A. Sánchez-Gil, M. Kuttge, P. Haring Bolívar, and H. Kurz, "Optically switchable mirrors for surface plasmon polaritons propagating on semiconductor surfaces," Phys. Rev. B **74**(24), 245324 (2006).
30. H.-T. Chen, W. J. Padilla, J. M. O. Zide, A. C. Gossard, A. J. Taylor, and R. D. Averitt, "Active terahertz metamaterial devices," Nature **444**(7119), 597–600 (2006).
31. H.-T. Chen, W. J. Padilla, M. J. Cich, A. K. Azad, R. D. Averitt, and A. J. Taylor, "A metamaterial solid-state terahertz phase modulator," Nat. Photonics **3**(3), 148–151 (2009).
32. V. Giannini, J. A. Sánchez-Gil, J. V. García-Ramos, and E. R. Méndez, "Collective electromagnetic emission from molecular layers on metal nanostructures mediated by surface plasmon," Phys. Rev. B **75**(23), 235447 (2007).
33. P. Mühlschlegel, H.-J. Eisler, O. J. F. Martin, B. Hecht, and D. W. Pohl, "Resonant optical antennas," Science **308**(5728), 1607–1609 (2005).
34. V. Giannini, and J. A. Sánchez-Gil, "Calculations of light scattering from isolated and interacting metallic nanowires with arbitrary cross section by means of Green's theorem surface integral equations in parametric form," J. Opt. Soc. Am. A **24**(9), 2822–2830 (2007).
35. O. L. Muskens, V. Giannini, J. A. Sánchez-Gil, and J. Gómez Rivas, "Optical scattering resonances of single and coupled dimer plasmonic nanoantennas," Opt. Express **15**(26), 17736–17746 (2007).
36. M. van Exter, and D. Grischkowsky, "Carrier dynamics of electrons and holes in moderately doped silicon," Phys. Rev. B **41**(17), 12140–12149 (1990).
37. S. Adachi, "Optical Constants of Crystalline and Amorphous Semiconductors: Numerical Data and Graphical Information," Springer-Verlag, (1999).
38. M. Ordal, L. Long, R. Bell, S. Bell, R. Bell, R. Alexander, Jr., and C. Ward, "Optical properties of the metals Al, Co, Cu, Au, Fe, Pb, Ni, Pd, Pt, Ag, Ti, and W in the infrared and far infrared," Appl. Opt. **22**(7), 1099–1119 (1983).
39. B. J. Messinger, K. U. von Raben, R. K. Chang, and P. W. Barber, "Local-fields at the surface of noble metal microspheres," Phys. Rev. B **24**(2), 649–657 (1981).
40. M. Thomas, J.-J. Greffet, R. Carminati, and J. R. Arias-Gonzalez, "Single-molecule spontaneous emission close to absorbing nanostructures," Appl. Phys. Lett. **85**(17), 3863–3865 (2004).
41. G. W. Bryant, F. J. García de Abajo, and J. Aizpurua, "Mapping the Plasmon Resonances of Metallic Nanoantennas," Nano Lett. **8**(2), 631–636 (2008).
42. P. J. Schuck, D. P. Fromm, A. Sundaramurthy, G. S. Kino, and W. E. Moerner, "Improving the mismatch between light and nanoscale objects with gold bowtie nanoantennas," Phys. Rev. Lett. **94**(1), 017402 (2005).
43. L. Novotny, "Effective Wavelength Scaling for Optical Antennas," Phys. Rev. Lett. **98**(26), 266802 (2007).

1. Introduction

The development of compact sources of terahertz (THz) electromagnetic radiation is consolidating emerging applications in this frequency range [1–3]. Simultaneously, the

growing interest in the field of plasmonics is converging to the THz regime [4–9]. Typical wavelengths corresponding to THz frequencies are in the range 30 μm (10 THz) to 3000 μm (0.1 THz), hence impairing spatial resolution for most applications. Moreover, the power of the available table top THz sources is still rather low, thus limiting applications in which high intensities are needed. Therefore, the large field confinement and enhancement that plasmonic surfaces can offer may be critical for the development of novel application of THz radiation [8, 9]. THz plasmonics have the potential to find natural applications in spectroscopic techniques for low concentration sensing, analysis and imaging of biological tissue and for security applications such as sensitive detection of explosives, drugs, chemical and biological agents [3].

Surface plasmon polaritons (SPPs) are electromagnetic waves bound to the surface of a conductor. These waves arise from the coupling of light to collective oscillations of the electronic charge density [10]. This coupling or, in other words, the confinement of the wave to the surface is maximal for frequencies close to the plasma frequency of the conductor and decreases as the frequency is reduced [11]. The plasma frequency of metals is typically in the visible or ultraviolet part of the electromagnetic spectrum and the confinement of SPPs to the metal at low frequencies, i.e., at THz frequencies, is very weak, as the waves evolve from a confined SPP to a delocalized Sommerfeld-Zenneck wave. Two major approaches can be employed to increase the confinement of THz SPPs: either electromagnetic waves bound to metal surfaces that mimic surface plasmon polaritons (referred to as spoof SPPs) are obtained by perforating a flat metal surface periodically with holes and grooves [12–18]; or SPPs are excited in surfaces, wires or particles, made of semiconductor instead of metal [19-20]. Semiconductors have a much lower plasma frequency than metals, typically in the mid-infrared, allowing the strong confinement of THz SPPs to their surface. Another crucial difference between metals and semiconductors is that semiconductors are much more versatile materials since their plasma frequency, hence the properties of SPPs, are remarkably tuneable. Switching of the SPP-assisted resonant terahertz transmission through hole arrays has been demonstrated using magnetic, electric, optical, and thermal techniques [21–26]. Also the propagation and scattering of THz SPPs on semiconductors [27–29] and the response of metamaterials [30, 31] have been actively modified. Consequently semiconductors are promising candidates for active plasmonic devices at THz frequencies.

In this paper we investigate theoretically localized surface plasmon resonances (LSPRs) at THz frequencies in indium antimonide (InSb) gap antennas formed by two closely spaced particles. We have focused our study on InSb antennas due to its large carrier mobility, which favors the excitation of LSPRs. InSb is a direct semiconductor with a small bandgap and a relatively high density of thermally excited free carriers at room temperature. LSPRs are identified in the far-field as resonances in the scattering cross section and in the near-field as maxima in the local enhancement factor of the electric field [32, 33]. In this study we have optimized the dimensions of dimer antennas to provide large enhancements around 1 THz in the antenna gap between the two particles. In analogy to optical metal nanoantennas, the resonances shift to lower energy for smaller gaps and for longer antennas. Using semiconductor antennas the resonances can be tuned in frequency by two means: passively by acting on the geometry, or actively by controlling the free carrier concentration. The tuneable character of semiconductors translates directly into the tuneability of the near-field enhancement.

2. Theoretical model

We have used the full electromagnetic (EM) Green's integral equation formulation, modified to deal with surface profiles in parametric form to investigate THz dimer antennas. This method is very powerful to solve electromagnetic scattering problems of objects with arbitrary shape [34]. We consider the following scattering configuration (see Fig. 1): two infinitely long wires, i.e., translational invariant along the *y*-direction are placed close to each other at a distance Δ.
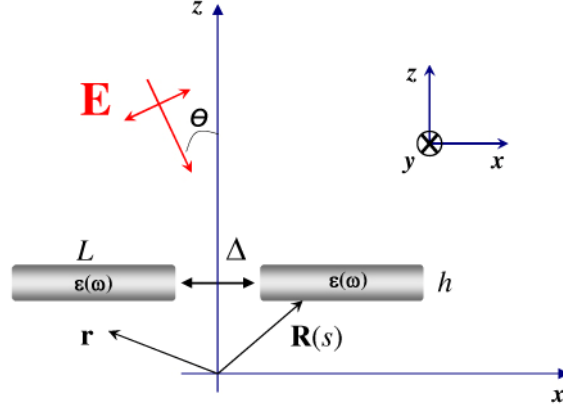
Fig. 1. Schematic representation of the scattering geometry. A monochromatic, linearly *p*-polarized incident beam impinges at an angle Θ on scatterers with frequency-dependent homogeneous permittivity ε. The distance between the scatters is Δ. **r** represents a generic point in the *(x, z)* plane and (**R**)(*s*) is a generic point on the parametric curve that delimitates each scatter.

This distance Δ is called the dimer gap. The incident electromagnetic field at THz frequency impinges at an angle θ with respect to the *z* axis, its electric field being in the *(x, z)* plane (*p*-polarization). The wires are defined by an isotropic and homogeneous frequency-dependent permittivity ε(ω). The restriction to wires with translational symmetry has the advantage that it notably simplifies the formulation; in fact, we can reduce the initial three-dimensional vectorial problem to a two-dimensional scalar one, where the EM field is entirely described in the case of *p*-polarization by the *y* component of the magnetic field. Applying Green's integral theorem, and proceeding as in Ref [34], we obtain the following system of coupled integral equations

$$H^{(i)}(\mathbf{r}) + \frac{1}{4\pi} \sum_j \int_{\Gamma_j} \left\{ H^{(out)}[\mathbf{R}_j(s)] \frac{\partial G^{(out)}[\mathbf{r},\mathbf{R}_j(s)]}{\partial N_j} - G^{(out)}[\mathbf{r},\mathbf{R}_j(s)] \frac{\partial H_j^{(out)}(\mathbf{R}_j(s))}{\partial N_j} \right\} ds = H^{(out)}(\mathbf{r}),$$

(1)

if **r** is outside Γ_j and

$$H^{(i)}(\mathbf{r}) + \frac{1}{4\pi} \sum_j \int_{\Gamma_j} \left\{ H^{(out)}[\mathbf{R}_j(s)] \frac{\partial G^{(out)}[\mathbf{r},\mathbf{R}_j(s)]}{\partial N_j} - G^{(out)}[\mathbf{r},\mathbf{R}_j(s)] \frac{\partial H_j^{(out)}(\mathbf{R}_j(s))}{\partial N_j} \right\} ds = 0,$$

(2)

if **r** is inside Γ_j.

The subscript *j* can take the values 1 or 2 and indicates the *j*-th wire, Γ_j represents the parametric curve that describes the *j*-th wire and $\mathbf{R}_j$(s) is a point on the parametric curve that delimitates wire. The superscripts *(out)* denotes that the magnetic field $H^{(out)}(\mathbf{r})$ is evaluated outside the wires. $H^{(i)}(\mathbf{r})$ is the incident field and $G^{(out)}(\mathbf{r},\mathbf{R})$ is the Green function of the system, and $\partial/\partial N$ is the normal derivative along the parametric curve. The function $G^{(out)}(\mathbf{r},\mathbf{R})$ is the Green function of free space and it is obtained from Helmholtz equations describing the magnetic field outside the scatterers. If translational symmetry is considered, the Green function is given by the zeroth-order Hankel function of the first kind. Similar expressions are obtained employing the Green's integral theorem inside the wires [34]. In this formulation, the electromagnetic field in the entire space is written as surface integrals of the EM fields at the interfaces separating domains with different permittivities. Such surface EM fields have to be determined by solving the system of surface integral equations obtained upon evaluating

the above integral equations at the interface for the corresponding incident field, exploiting, in turn, the continuity conditions.. Sampling each surface profile, we convert the systems of integral equations (Eqs. (1) and (2)) into a solvable linear numerical system. This formulation is rigorous from the standpoint of classical electrodynamics and has been successfully applied to study a variety of problems with reasonable approximations of the 3D case for particular geometries [35].

In order to describe the system fully, one needs to define the permittivity of the different domains. Time resolved THz studies of carrier dynamics (electrons and holes) in semiconductors [36] have shown that the permittivity function $\varepsilon(\omega)$ of semiconductors at THz frequencies is well described by the Drude model for free carriers

$$\varepsilon(\omega) = \varepsilon(\infty) - \frac{\omega_p^2}{\omega^2 + i\omega\gamma},$$ (3)

where $\varepsilon(\infty)$ is the high-frequency permittivity, $\gamma = 1/\tau$ is the carrier momentum relaxation rate and τ is the average collision time of the charge carriers. The momentum relaxation rate γ is related to the carrier mobility μ by

$$\gamma = m^*\mu / e ,$$ (4)

where m^* the effective mass of the charge carriers and e the elementary charge. The plasma frequency ω_p is defined as

$$\omega_p^2 = e^2 N / (\varepsilon_0 m^*),$$ (5)

where N is the free carrier concentration and ε_0 the vacuum permittivity. From the above expressions of the plasma frequency and momentum relaxation rate, it follows that the permittivity depends on the carrier concentration and the carrier mobility. Since these parameters can be varied in semiconductors in several ways, for example with chemical doping, by changing the temperature, by optical excitation of carriers to the conduction band or by electrical injection of carriers, the permittivity can be tuned. More details on the tuning properties of semiconductor THz antennas are given in section 3.3.

The complex permittivity of undoped InSb at 300K ($N = 2\cdot10^{16}$cm^{-3}) in the THz regime is displayed in Fig. 2(a), in which the real component is represented by the black squares and the imaginary component with the red circles [37]. Indium antimonide is a good candidate for THz plasmonic devices owing to its small energy band gap and large electronic mobility [20, 26–29]. The plasma frequency of InSb is in the THz range ($\omega_p/2\pi \approx 2.8$ THz). Therefore, the values of the permittivity of InSb at THz frequencies are similar to those of metals in the visible and near infrared, i.e., the permittivity has a real negative part with a small absolute value and a small imaginary component related to material losses. In contrast, the permittivity of gold (see Fig. 2(b)) at THz frequencies has very large negative real values and a large imaginary component. These values, several orders of magnitude larger than those of InSb, are due to the higher plasma frequency of gold compared to InSb ($\omega_p/2\pi \approx 2000$ THz) and to the ω^{-2} dependence of Eq. (3) [38].
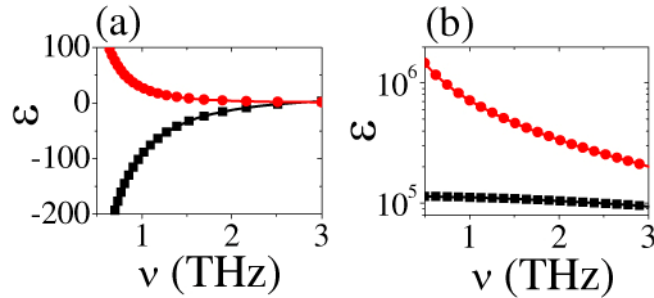
Fig. 2. Complex permittivity of InSb (a) at room temperature and of gold (b) at THz frequencies calculated using the Drude model. The black squares correspond to the real component of the permittivity (absolute value in (b)), while the red circles are the imaginary component.

The difference in plasma frequency between InSb and Au is mainly determined by the much higher free carrier density of metals (N_{Au} = 5.9·10^{22} cm^{-3}). Due to the similar permittivities of InSb at THz frequencies and gold in the visible, it is reasonable to expect localized plasmon resonances at THz frequencies on InSb antennas with scaled dimensions. In the next section we have investigated the scattering cross section and the THz near-field distribution of InSb dimer plasmonic antennas.

3. Plasmonics resonances in InSb antennas

3.1 Scattering cross sections

We have focused our study on the THz scattering properties of dimer plasmonics antennas as the one represented in Fig. 1. Dimer antennas are formed by two similar arms of length L and height h separated by a subwavelength gap Δ. We consider the interaction of a plane wave at THz frequencies impinging on the antenna at θ=0°. The incident field is p-polarized, i.e., the electric field is in the plane of the figure along the x-direction, i.e., parallel to the long axis of the antenna. From the far field scattered by the antennas we have calculated the scattering cross section (SCS) [34]. We have normalized the SCS to the geometrical cross section of the antenna, i.e., the antenna length L. This normalization provides an intuitive characterization of the strength of the interaction of the incident THz wave with the antennas.. For scattering cross sections bigger than the geometrical cross section, the energy of the incident field around the antenna is concentrated on the antenna, leading to a local enhancement of the electromagnetic field. In Fig. 3(a) the scattering cross section normalized to the antenna length L, i.e., the scattering efficiency (Q_{eff}), is shown for different lengths ranging from 30 μm to 70 μm. The gap width is 2 μm and the height of each dimer is 5 μm. As expected, the SCSs exhibit a resonance when the real part of the permittivity of InSb is negative and the imaginary part is relatively small, i.e., around 1.5 THz. These resonances are the lowest order plasmonic resonances, i.e., the semiconductor structure acts as half wavelength (λ/2) antenna. As in the case of metal nanoantennas [34, 35], the localized plasmon resonance shifts to lower frequencies as the antenna length is increased. The longest antenna with L=70μm (green triangles in Fig. 3(a)) exhibits a small shoulder around 2.2 THz due to a weak excitation of a higher order resonance, i.e., the 3λ/2 resonance.. Narrower resonance widths are found for shorter lengths due to a reduced radiative damping.

For comparison we have calculated the scattering efficiency of a gold antenna (Fig. 3 (b)) with identical geometrical parameters as the InSb antenna. Due to the huge values of the permittivity of gold at THz frequencies, the skin depth of gold is much smaller (some 10s of nm) than the antenna dimensions. Therefore, gold antennas can be approximated as perfect linear conductor antennas, which are resonant when the length of the antenna matches with multiples of half of the wavelength. In case of dimer antennas with a total length equal to $2L+\Delta$ and $\Delta \ll L$, this resonant condition can be written as $L \approx m\lambda/4n$, with n the refractive index of the surrounding medium and m a positive integer which indicates the resonance

order. Taking into account the symmetry of the antenna, when the light impinges on the top (see Fig. 1) only odd order resonances can be excited [34]. Thus, it is possible to approximate resonances in Fig. 3(b) with the odd m order given by the classical antenna theory.
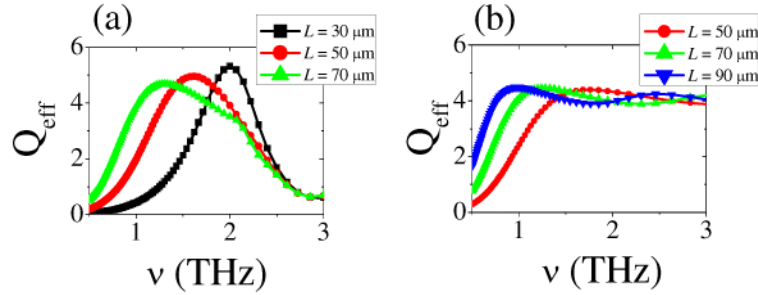

Fig. 3. Scattering efficiency of rectangular dimers (see Fig. 1) with different lengths L, illuminated with THz radiation polarized along L, the permittiviy of the background is one. The height h of the dimers is 5 µm and the gap Δ is 2 µm. The lengths are indicated in the figure legends. Figure (a) corresponds to calculations of InSb dimer antennas, while the calculation of (b) corresponds to gold antennas.

An important difference between InSb and gold antenna resonances is their shape. In the case of gold, the first order and higher order resonances overlap resulting in a smoothed spectrum. Furthermore, it is possible to excite resonances at frequencies higher than 3 THz in gold antennas (not show in Fig. 3), whereas in InSb at room temperature there are resonances only below ~3 THz, i.e., below the semiconductor plasma frequency where InSb has a metallic character.

3.2 Near-fields

In order to further elucidate the differences between plasmonic resonances in InSb antennas and resonances in gold antennas, we have calculated the corresponding near-field patterns. Figure 4 displays the near-electric-field intensity distribution for a resonant antenna of InSb (Fig. 4(a)) and of Au (Figs. 4(b)) with the same dimensions, L=50µm, Δ=2µm and h=5µm. The near-fields have been calculated at their respective resonance frequencies, i.e., 1.62 THz for the InSb antenna and at 1.73 THz for the Au antenna. The near-field intensities of Fig. 4 have been normalized to the incident field and plotted in logarithmic scale to distinguish the highest enhancements in the gap. Figures 4(c) and (d) represent the near-field enhancement along a line through the middle of the InSb (Fig. 4(c)) and Au (Fig. 4(d)) antenna parallel to its long axis. The near-fields present several similarities: there are maxima in the enhancement at the edges of the antenna and in the antenna gap. These maxima are caused by the coexistence of two effects: the lightning rod effect at the sharp corners and by the localized plasmon resonance. The gap enhancements are almost uniformly distributed inside the gap. This can be better appreciated in the zooms around the gap displayed in Figs. 4(e) for InSb and Fig. 4(f) Au. Quantitatively, the enhancement factors at the center of the gap are larger for InSb (~95) than those for Au (~75), highlighting the relevance of LSPRs in semiconductor antennas. For a gap size of 2 µm as displayed on Fig. 4, the field enhancement is increased by a factor of 1.25 when choosing semiconductors. The main difference in the near-field is found inside the antennas themselves. Due to the large value of the permittivity of gold, the electric field does not penetrate inside the antenna and the field vanishes in contrast to the finite field in the InSb antenna. The enhancements in Fig. 4 and 5
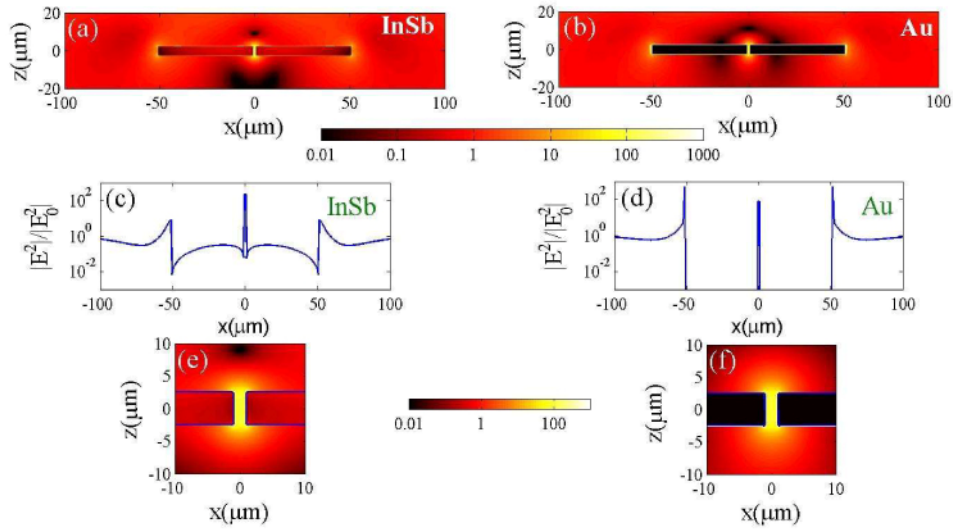
Fig. 4. Near-field intensity distribution in logarithmic scale at the main resonance. (a) InSb (N=2·10^{16} cm^{-3}) antenna with a gap Δ=2 μm, length L=50 μm, height h=5 μm and ν=1.62 THz. (b) Au antenna with same dimension as (a) but at ν=1.73 THz. (c) Horizontal cut of (a) at z=0. (d) Horizontal cut of (b) at z=0. (e) Zoom around the gap of (a). (f) Closed view of the gap of (b). The amplitude of the incident plane wave is one and impinges from the top at θ=0° (see of Fig. 1), the permittivity of the background is one.

are calculated at the resonant frequency obtained from the SCS spectrum. It should be pointed out that when retardation effects are important the largest near-field enhancement is at a frequency slightly shifted with respect to the far field resonance [39–41].

It is interesting to determine the field enhancement in the gap as a function of the geometrical parameters of the antenna at a given frequency. These calculations serve as guideline to design plasmonic THz antennas with optimized enhancements for, e.g., sensing applications. Figure 5 shows the result of this calculation at 1.5 THz varying the gap and length of the dimer. Similarly to what is found for metal nanoantennas, larger enhancements are found for smaller gaps due to the capacitive coupling of the arms of the dimer. From Fig. 5, the largest enhancement factors are obtained for an antenna of length 40 μm. However, Fig. 3 (a) indicates that the resonance peak in the SCS is around 1.5 THz for an antenna length larger than 50 μm. This difference highlights the aforementioned frequency shift between the near-field plasmonic resonance and the far-field resonance in the SCS.
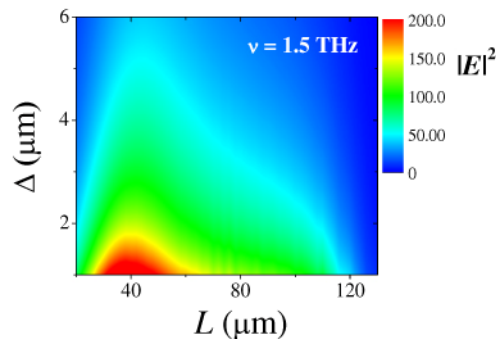

Fig. 5. Near-field intensity enhancement at the central point of the gap of a rectangular dimer InSb antenna with an electron concentration N=2·10^{16}cm^{-3} as a function of the antenna length L and gap Δ. The height of the antenna is 5 μm. The electric field (p-polarized plane wave) impinges on the top at ν = 1.5 THz. The permittivity of the background is one.

Rectangular gap dimers are probably the simplest structures with large enhancement factors that can be understood from classical antenna theory. However, more complex structures can yield larger enhancements. An example of these structures is the bowtie antenna, which has been recently investigated in the optical regime [42]. An example of an InSb bowtie antenna is displayed in Fig. 6. A bowtie antenna is formed by two triangular particles symmetrically placed and oriented so that the triangle base is perpendicular to the dimer axis and with the apex pointing towards the gap. The bowtie antenna of Fig. 6 has a height of 20 µm, a base of 20 µm and a gap width of 1 µm. The electric field impinges on the top at the resonant frequency 2.1 THz. The near-field intensity distribution is displayed in Fig. 5(a) and the enhancements along the main axis at $z=0$ are shown in Fig. 5(b). For this particular antenna we can achieve enhancements factors larger than 10^3 in the gap.
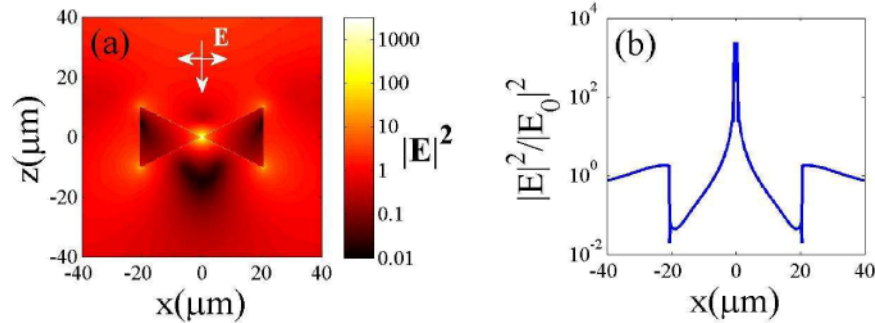

Fig. 6. (a) Near-field intensity distribution in logarithmic scale at the plasmonic resonance ($v = 2.1$ THz) of an InSb bowtie antenna, the permittivity of the background is one. Each triangle of the bowtie has the base and height with a length of 20 µm and the gap is $\Delta=1$ µm. The incident field, with an amplitude equal to one and a frequency of 2.1 THz, impinges from the top as illustrated by the white arrow. The perpendicular double arrow indicates the polarization. (b) Near-field intensity at $z=0$.

3.3 Tuneability of semiconductor THz antennas

An important advantage of semiconductors over metals for THz plasmonics is the possibility to tune their permittivity by controlling the concentration of free carriers. This control can be achieved passively by changing the semiconductor dopant density or actively by injecting carriers, e.g., thermally, optically or electrically, from the valence band or from impurity levels to the conduction band..

Considering the optimized dimensions within the calculated range for an InSb rectangular antenna to support a LSPRs at 1.5 THz, i.e., $L=40$µm and $h=5$µm (see Fig. 5), we have explored the tuneable properties of this resonance upon variation of the carrier concentration. Figure 7(a) shows the near-field enhancement at the central point of dimer gap as a function of the free-electron concentration. The calculations are done at room temperature, using a carrier and temperature dependent mobility [37], and for different dimensions of the gap $\Delta = 0.1$ μm (down blue triangles), 0.2 μm (up green triangles), 0.5 μm (red circles), and 1.0 μm (black squares). A minimum in the intensity enhancement appears for $N = 6 \cdot 10^{15}$ cm^{-3}. Below this value modest enhancements are obtained. A rapid increase in the enhancement is observed for values of the carrier concentration above $6 \cdot 10^{15}$ cm^{-3}, with a local maximum around $N = 2 \cdot 10^{16}$ cm^{-3} and a decrease of the enhancement for larger N. This behavior can be understood by looking to the value of the permittivity of InSb at 1.5 THz as a function of the carrier concentration. This value is represented in Fig. 7(b), where the blue triangles are $-\text{Re}(\varepsilon)$ and the red circle are $\text{Im}(\varepsilon)$. The real component of the permittivity is negative, i.e., InSb behaves as a conductor, only above $N \sim 6 \cdot 10^{15}$ cm^{-3}. For this carrier concentration the plasma frequency is 1.5 THz. The permittivity of InSb has positive real component and a small imaginary component for $N < 6 \cdot 10^{15}$ cm^{-3}, i.e., InSb behaves as a dielectric and no large enhancements are expected. Above $N \sim 6 \cdot 10^{15}$ cm^{-3}, as the imaginary component of the

permittivity increases, the excitation of surface plasmon resonances is less efficient due to larger Ohmic losses. Therefore, the most favorable carrier concentrations are below $N \sim 10^{17}$ cm^{-3}. If the free carrier concentration is further increased, InSb approaches the perfect conductor limit behaving as a metal at THz frequencies. In this limit, the enhancements are lower and due to the lightning rod effect at the corners of the antenna. The dependence of the enhancement with carrier concentration does not change qualitatively when the dimension of the gap is varied (see Fig. 7 (a)). Only the enhancement increases inversely proportional the size of the gap. Note that the strong dependence of the field enhancement with carrier concentration, which in turn can be easily controlled in semiconductors, represents an important step towards active plasmonics functionalities.
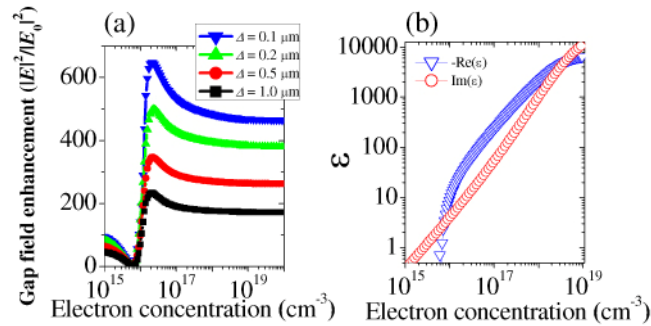

Fig. 7. (a) Near-field intensity enhancement at middle position of the gap, of an InSb dimer antenna as a function of the electron concentration. The antenna dimensions are h=5 μm, and L=40 μm with different gap widths dimensions Δ. A plane wave of frequency ν = 1.5 THz and polarized along L impinges on the top of the antenna (θ=0°).,The permittivity of the background is one. (b) Minus the real component (blue triangles) and the imaginary component of the complex permittivity of InSb at ν = 1.5 THz as a function of the electron concentration.

Let us now turn our attention to the far field resonances and discuss their behavior as a function of the free-carrier concentration. The calculation of the scattering efficiencies as a function of frequency for different carrier concentrations is displayed in Fig. 8. These efficiencies are computed for a dimer InSb antenna with dimensions L = 40 μm, h = 5 μm, and gap width Δ = 1 μm. The dimensions of the antenna are chosen to optimize the field enhancement in the gap at 1.5 THz. A p-polarized electromagnetic wave field impinges on top. The LSPRs for a low carrier concentration evolves into a broader resonance as the carrier concentration is increased. Also the resonant frequency shifts to higher frequencies, from ~1 THz to ~2 THz, as the carrier concentration increases from 10^{16} to 10^{17} cm^{-3}. We can understand this behavior by considering the dependence of the permittivity and the plasma frequency on the carrier concentration. By increasing the carrier concentration the plasma frequency shifts to higher values. This, in turn, increases the frequency of the LSPR [43]. Moreover, a higher plasma frequency gives rise to a larger imaginary component of the permittivity at the resonance frequency, hence an increase of losses which broadens the resonance.
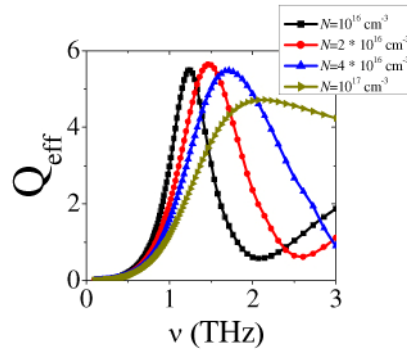
Fig. 8. Scattering efficiency of an InSb dimer antenna for various electron concentrations, The dimer has a gap Δ=1 μm, a length L=40 μm and a height h=5 μm, and it is illuminated from the top (θ=0°) with a plane wave polarized along L. The permittivity of the background is one.

4. Conclusion

We have theoretically investigated localized surface plasmon resonances in semiconductor antennas in the terahertz regime. It was shown that InSb dimer antennas with appropriate dimensions exhibit plasmonic resonances with large enhancement factors (10^2-10^3 times the incident field). The achieved field enhancement is larger than that obtained with gold dimer antennas with identical dimensions due to the enhanced plasmonics character of semiconductors at THz frequencies. These antennas are the analogue at THz frequencies of metal plasmonic nanoantennas in the visible. Moreover, semiconductor based THz antennas are more versatile than their metallic counterparts since the dielectric properties of semiconductors depend on the free-carrier concentration and mobility. These parameters can be controlled in several ways, e.g., by changing temperature, doping concentration, applying an electric potential or by optical pumping. The control of the permittivity allows active tuning of plasmonic resonances and enhancement factors. Therefore, semiconductor dimer antennas are excellent candidates for applications in which large THz field enhancement and active control of these enhancements are required. These applications can be found in THz spectroscopy and sensing of low concentrations and in THz modulators.

Acknowledgements